Zhong et al. Nanoscale Research Letters (2017) 12:533
DOI 10.1186/s11671-017-2305-4

Nanoscale Research Letters

NANO IDEA Open Access

Successive Release of Tissue Inhibitors of Metalloproteinase-1 Through Graphene Oxide-Based Delivery System Can Promote Skin Regeneration

Cheng Zhong[1], Dike Shi[2], Yixiong Zheng[2], Peter J. Nelson[3] and Qi Bao[4,5*]

Abstract

The purpose of this study was to testify the hypothesis that graphene oxide (GO) could act as an appropriate vehicle for the release of tissue inhibitors of metalloproteinase-1 (TIMP-1) protein in the context of skin repair. GO characteristics were observed by scanning electron microscopy, atomic force microscopy, and thermal gravimetric analysis. After TIMP-1 absorbing GO, the release profiles of various concentrations of TIMP-1 from GO were compared. GO biocompatibility with fibroblast viability was assessed by measuring cell cycle and apoptosis. In vivo wound healing assays were used to determine the effect of TIMP-1-GO on skin regeneration. The greatest intensity of GO was 1140 nm, and the most intensity volume was 10,674.1 nm (nanometer). TIMP-1 was shown to be continuously released for at least 40 days from GO. The proliferation and viability of rat fibroblasts cultured with TIMP-1-GO were not significantly different as compared with the cells grown in GO or TIMP-1 alone ($p > 0.05$). Skin defect of rats treated with TIMP-1 and TIMP-1-GO showed significant differences in histological and immunohistochemical scores ($p < 0.05$). GO can be controlled to release carrier materials. The combination of TIMP-1 and GO promoted the progression of skin tissue regeneration in skin defect.

Keywords: Graphene oxide, TIMP-1, Successive release, Skin regeneration

Background

Skin lesions can be caused by many factors such as accidents, diabetic complications, burns, or superficial surgery [1]. Autogenous skin transplantation, or biopolymers used for fabrication of the artificial skin, represents the most common approach used for wound closure [2]. These substitutes can include a limitation of available donor soft tissue, especially in severely burned patients [3], infection [4], pain, and skin flap necrosis [5], slowing healing and biocompatibility of the material.

Tissue inhibitor of metalloproteinase-1 (TIMP-1) prevents the extracellular matrix (ECM) from being decomposed by forming an inhibitory complex with the matrix metalloproteinases (MMPs) [6, 7]. TIMP proteins also control the MMP-driven turnover and processing of growth factors as well as cytokines linked to wound repair and regeneration [8]. TIMPs and MMPs are regulated during normal wound healing, and their imbalance has been implicated in skin repair defects, keloids, and fibrosis [9]. Epithelial-derived TIMP-1 can regulate epithelialization in different stages either directly or indirectly. An important phase of excisional wound repair and skin regeneration is re-epithelialization, which is the re-growth of epithelia over a traumatic surface [10]. Re-epithelialization occurs when cells at the wound margin loosen their cell–cell and cell–ECM contacts and begin to migrate across the wound. These processes have been linked to TIMP-1 biology [11].

An optimal regional TIMP-1 administration system for the restoration of the skin is dependent on the delivery vehicle used. Some delivery vehicles designed to release cytokines have been developed [12]. Carriers

* Correspondence: baoqi@zju.edu.cn
[4]Department of Plastic and Reconstructive Surgery, Second Affiliated Hospital, School of Medicine, Zhejiang University, Hangzhou, China
[5]Institute of Gastroenterology, Zhejiang University, Hangzhou, China
Full list of author information is available at the end of the article

Springer Open

© The Author(s). 2017 **Open Access** This article is distributed under the terms of the Creative Commons Attribution 4.0 International License (http://creativecommons.org/licenses/by/4.0/), which permits unrestricted use, distribution, and reproduction in any medium, provided you give appropriate credit to the original author(s) and the source, provide a link to the Creative Commons license, and indicate if changes were made.

include PLGA (poly(lactic-co-glycolic acid)) [13], chitosan [14], PLGA nano-spheres [15], and hydrogels. The use of a delivery vehicle would help reduce the TIMP-1 dosage for skin regeneration and allow a regional delivery of the agent. Graphene is composed of carbon atoms with a flat monolayer and a honeycomb-like two-dimensional structure [16]. Graphene oxide (GO) has been used as a small molecule drug delivery vehicle in literature as it has efficient loading (absorption), is biocompatible, and has low toxicity [17–19]. Essential characteristics of GO include hydrophobic π domains in the core of the structure with ionized regions along the edges. The distinctive $\pi-\pi$ stacking interaction makes GO efficient with water solubility, with a large specific surface area for high loading capacity [20, 21].

In the present study, we have investigated whether recombinant human TIMP-1 protein can be paired with GO as a delivery vehicle to improve skin regeneration. To investigate the effect on skin regeneration, TIMP-1 has been loaded onto GO flakes, and its release and toxicity are measured in vitro via rat fibroblasts. The results are finally tested on rats where a skin wound model is used.

Materials and Methods

Cell Culture

Rat fibroblasts were purchased from the Institute of Biochemistry and Cell Biology, CAS (Shanghai, China), and cultured in Dulbecco's modified Eagle's medium (DMEM, GibcoBRL, Gaithersburg, MD, USA) containing 10% (*v*/*v*) fetal bovine serum (FBS, Gibco). The medium was changed every 2 days. All the cells were kept at 37 °C.

GO Characterization

GO flakes were purchased from Chengdu Organic Chemicals Co., Ltd. Chinese Academy of Science (Chengdu, China) and characterized using scanning electron microscopy (SEM, JSM-6701F, JEOL, Tokyo, Japan) after platinum coating. The samples were scanned under a scanning electron microscope (Hitachi S3000N) at 15 kV accelerating voltage. The size distribution of the GO flakes was determined with a zeta electric potential-based spectrophotometer (Zetasizer 3000 HSA, Malvern, UK). The morphology of the GO flakes was determined using atomic force microscopy (AFM, MultiMode, VEECO, USA) coupled with an inverted microscope (IX71 inverted microscope, Olympus, Tokyo, Japan). Thermal gravimetric analysis and differential scanning calorimetry were performed using a TGA/DSC thermogravimetric analyzer (Pyris 1 TGA, Perkin-Elmer, USA) by placing the samples in alumina pans and applying a heating ramp from 25 to 1100 °C at 10 °C/min.

TIMP-1 Adsorption on GO

GO flakes were labelled with 1,1-dioctadecyl-3,3,3,3-tetram-ethylindocarbocyanine perchlorate (DiI, red, Sigma) before human recombinant TIMP-1 (Huaan Co., Hangzhou, China) adsorption. For TIMP-1 adsorption, fluorescein isothiocyanate (FITC, green, Thermo Scientific, Rockford, IL, USA)-conjugated TIMP-1 (Huaan Co., Hangzhou, China) and DiI-labeled GO were added to phosphate-buffered saline (PBS) and incubated for 4 h at 4 °C. The ratio of GO to recombinant TIMP-1 was 1:1 by weight. To determine the TIMP-1 loading on GO, TIMP-1 (1 μg) was added to 20 μl of PBS containing GO and incubated for 4 h at 4 °C. TIMP-1 adsorbed to GO was visualized using a laser scanning confocal microscope (IX81-FV1000 inverted microscope, Olympus). To confirm TIMP-1 adsorption onto GO, Fourier-transformed infrared spectroscopy (FTIR) was performed using a Nicolet 5700 spectroscopy (ThermoFisher Co., SGE, Australia) on pellets (10 mm in diameter) prepared by blending 2 mg GO with 100 mg KBr and pressing to produce the pellet to be analyzed. Spectra were analyzed after baseline correction by the software EZ OMNIC (Nicolet).

Release Kinetics of TIMP-1 Protein

The release profiles of TIMP-1 from various GO concentrations (10, 20, and 30 μg/ml) were determined using a commercial human TIMP-1-specific enzyme-linked immunosorbent assays (ELISAs, R&D Systems Inc., Minneapolis, MN, USA). Following incubation for 4 h at 4 °C, an ELISA of the supernatant showed that virtually all the TIMP-1 was adsorbed on the GO. The TIMP-1-loaded GO was suspended in 60-mm culture dishes containing 1.5 ml PBS. The dishes were then incubated at 37 °C. At various time points, the supernatant was collected after continuous agitation and fresh buffer was added to the culture dishes. The concentration of human TIMP-1 in the supernatant was determined by ELISA.

GO Biocompatibility Assay

Twenty micrograms per milliliter GO flakes loaded with a 20 μg/ml concentration of TIMP-1 were added to rat fibroblast cultures, and the cells were cultured for 6, 24, 48, and 72 h. Cell viability was evaluated by using the cell counting-8 (CCK8) assay as described in manufacturer's instruction. The absorbance of the sample was expressed as absorbance value at 450 nm (n = 5 for each group).

Flow Cytometric Characterization

Fibroblasts were harvested by trypsinization and labeled with Hoechst 33258 and Annexin-V-FITC/PI. Cell cycle activity and cell apoptosis were subsequently determined by flow cytometry analysis kit (Lianke, Hangzhou, China). Labeling was performed for 30 min at 4 °C in the presence of blocking reagent (Lianke, Hangzhou, China), followed by two washing steps using PBS. After washing and fixing, at least 10^4 cells were acquired and analyzed. Flow cytometric analysis was performed using a Becton Dickinson FACSCanto II.

In Vivo Experiment

All experimental procedures were conducted according to the guidelines of the NIH in the USA. The animals for experimental procedures were approved by the Zhejiang University Ethics Committee. Four-week-old male Sprague–Dawley rats were administered skin defect surgery (SDS) as described previously (Fig. 4a) [22]. The size of skin defection was 10 mm × 10 mm. After the surgery, the animals were returned to their individual cages. Fourteen days after SDS, the animals were randomly divided into four groups and therapy was initiated. Local injections of control agent (4 ml PBS only), GO agent (4 ml GO with PBS, 1:20), TIMP-1 agent (4 ml TIMP-1 with PBS 1:20), or TIMP-1-GO agent (4 ml GO with TIMP-1, 1:1 *v*/*w*) were administered subcutaneously. The injections were made every week around the skin defect (a total of 4 points, 1 ml each) for a total of two treatments over a span of 2 weeks. The rats were sacrificed 4 weeks after surgery (Fig. 4a). The regenerated skin was dissected, embedded in paraffin, and investigated by hematoxylin–eosin staining and Masson staining.

Histological and Immunohistochemical Analysis

The regenerated skins were fixed in 4% formalin for 72 h. Then, the samples were decalcified in 9% formic acid for 2 weeks at room temperature. The samples of skin were dehydrated by graded ethanol. The consecutive sections were stained with hematoxylin–eosin (HE) and Masson. Expression of CD34 at the skin defect was analyzed by immunohistochemical staining. The sections were dewaxed in xylene and hydrated through graded alcohols. After blocking with 1% goat serum (1:100 dilution, Sigma), the sections were incubated with primary antibodies against CD34 (Abcam, Cambridge, UK) overnight at 4 °C. After washing with PBS for three times, the sections were incubated with secondary antibody for 1 h at 37 °C. Staining was developed with 3,3′-diaminobenzidine (DAB) solution (Dako, Hamburg, Germany). The regenerated skin was observed by three trained observers. The immunohistochemical sections were staged using the percentage of DBA.

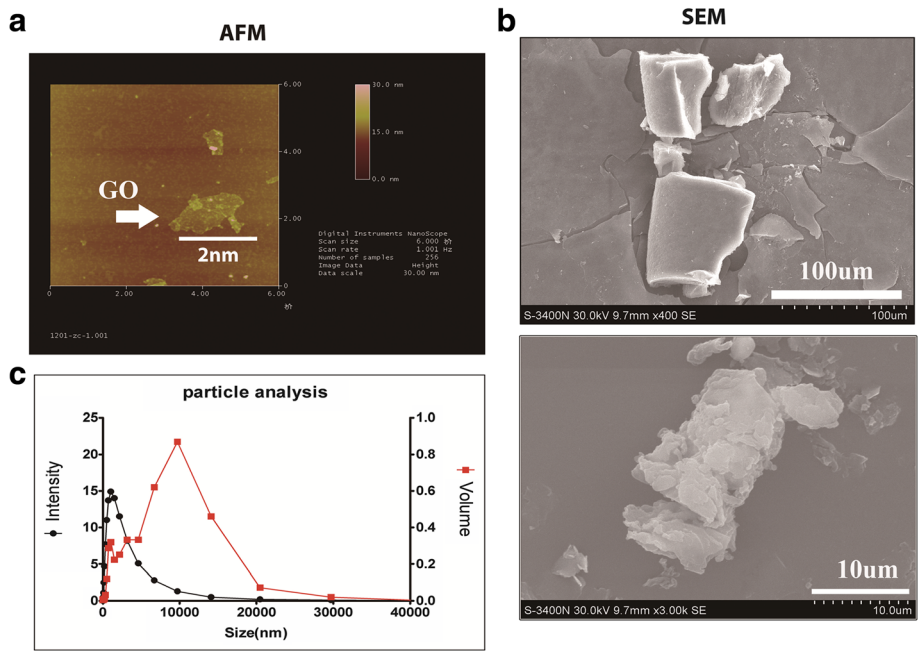

Fig. 1 GO absorption. **a** 2D representation of GO images showed at AFM. **b** SEM shows that GO flakes are irregularly shaped sheets. The GO flakes were irregularly shaped sheets. **c** The size distribution of the GO flakes. The greatest intensity was 1140 nm and the most intensity volume was 10,674.1 nm

Statistical Analysis

All experiments were repeated three times, and the data were presented as means ± standard deviation. One-way ANOVA and the Student–Newman–Keuls post hoc test determined the level of significance. p values which are less than 0.05 and 0.01 were respectively considered to be significant and highly significant. Statistical analysis was performed with SPSS 17.0 (SPSS Inc., Chicago, USA).

Results

GO Characterization

The 2D representation of GO images is showed at AFM (Fig. 1a). A SEM showed that the GO flakes were irregularly shaped sheets (Fig. 1b). The size distribution of the GO flakes was measured by an electric potential-based spectrophotometer. The greatest intensity of size distribution was 1140 nm, and the most intensity volume of the GO was 10,674.1 nm (Fig. 2a).

TIMP-1 Adsorption on GO

Following is the incubation of FITC-conjugated TIMP-1 (green) and DiI-labeled GO (red) in PBS for 4 h; TIMP-1 was adsorbed onto the GO. The analysis revealed that 75 ± 1.2% of GO was absorbed to TIMP-1 after 4 h, which suggested that GO efficiently binds to TIMP-1 protein (Fig. 1c). We investigated the chemical composition of TIMP-1-GO using FTIR spectroscopy (Fig. 2b). The waveform and the wave peak of GO were significantly different from those of TIMP-1-GO. We further investigated the thermal gravimetric analysis between control GO and TIMP-1-GO (Fig. 2d). The curve of thermal gravimetric analysis showed no appreciable differences between control GO and TIMP-1-GO.

TIMP-1 Release

Various concentrations of TIMP-1 (group 1 3 μg/ml, group 2 2 μg/ml, and group 3 10μg/ml) were loaded onto GO. The cumulative release profiles of TIMP-1 are shown in Fig. 2c. The 2 μg/ml TIMP-1-GO release reached 50% cumulative release more rapidly as compared to the 10 and 30 μg/ml TIMP-1 dose. TIMP-1 was continuously released for about 40 days. This suggests that the application of TIMP-1 embedded in GO may represent a suitable system for prolonged TIMP-1 release (Fig. 2c).

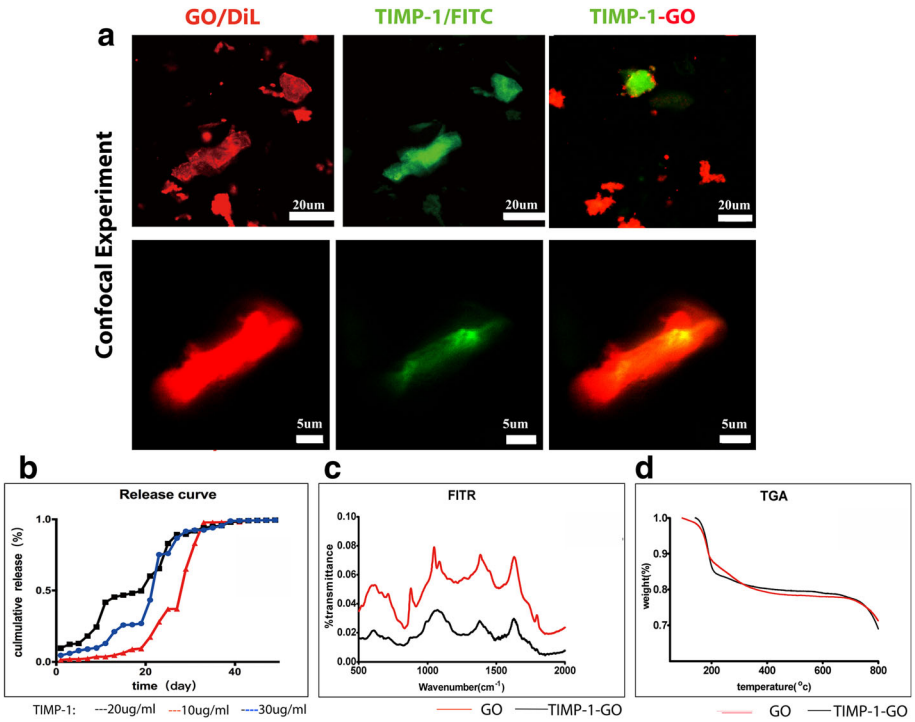

Fig. 2 GO and TIMP-1-GO characterization. **a** TIMP-1 was absorbed onto GO. The analysis revealed that 75 ± 1.2% of GO was absorbed to TIMP-1. **b** The cumulative release profiles of TIMP-1 were recorded. TIMP-1 embedded in GO represents a suitable system for prolonged TIMP-1 release about 40 days. **c** The chemical composition between the GO and TIMP-1-GO was investigated using FTIR spectroscopy. The waveform and the wave peak of GO were significantly different from those of TIMP-1-GO. **d** The curve of thermal gravimetric analysis shows no major differences between GO and TIMP-1-GO from 50 to 800 °C. The curve of thermal gravimetric analysis showed no appreciable differences between control GO and TIMP-1-GO

Cell Proliferation and Viability on TIMP-1-GO

The proliferation and viability of rat fibroblasts cultured in control, GO and TIMP-1, were not appreciably different than those of the cells grown in the different samples of TIMP-1-GO ($p > 0.05$). The cell cycle and apoptosis of fibroblasts cultured in control, GO and TIMP-1, were not appreciably different than that of cells grown in the samples of TIMP-1-GO ($p > 0.05$) (Fig. 3a–c).

Efficacy of TIMP-1-GO in Excisional Skin Wound Model

TIMP-1-GO was administered subcutaneously to rats to determine whether it could promote healing of the experimental wound. Four weeks after surgery, in comparison with control group, skin defects treated with TIMP-1-GO showed significant differences in terminal point ($p < 0.05$), while skin defects treated with TIMP-1 showed significant differences with the control group and GO group in terminal point ($p < 0.05$). Furthermore, the TIMP-1-GO group exhibited an enhanced therapeutic effect in hair follicles regeneration ($p < 0.05$). Skin defects treated with TIMP-1 showed significant differences with control group and GO group in terminal point ($p < 0.05$) (Fig. 4b).

Histologic and Immunohistochemical Analysis

Histologic features of skin regeneration after treatment with PBS are displayed in Fig. 4b. The features in control groups after skin defect show broken collagen fiber visible in the specimens 4 weeks after treatment. In contrast, continuous collagen fiber is visible in the TIMP-1-GO groups at the same time point and shows a statistical difference compared with the control group. Immunohistochemical features of vascularization after treatment of TIMP-1-GO are displayed in Fig. 3c. CD34+ subcutaneous cells are visible in the specimens after 4 weeks in the TIMP-1-GO-treated groups. The quantitative assessment revealed significant differences between the control groups and the TIMP-1-GO treatment group ($p < 0.05$) (Fig. 4c).

Discussion

In the present study, we have analyzed a potential new approach for enhancing excisional wound repair by combining recombinant TIMP-1 protein with controlled release from GO. GO has showed good biocompatibility in vitro. And TIMP-1 is shown to be continuously released from the GO vehicle for up to 40 days. The combination of TIMP-1 with GO is

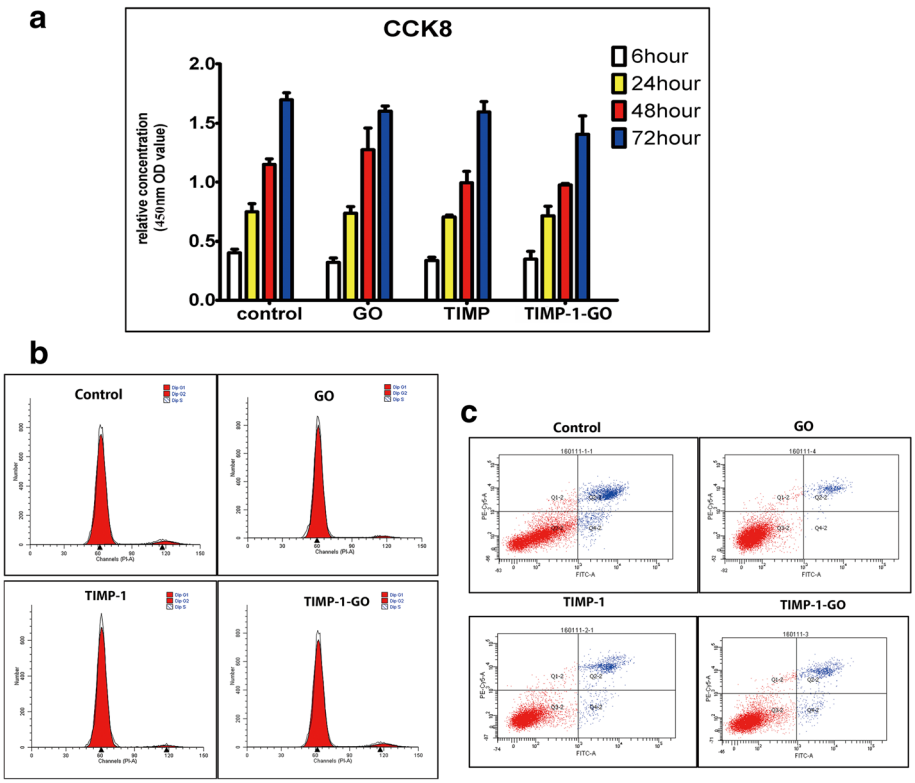

Fig. 3 The effect of TIMP-1-GO on rat fibroblast cell proliferation and viability. **a** The viability of fibroblasts cultured in different groups show no significant differences in different time points ($p > 0.05$). **b** The cell cycle of fibroblast was not significantly different than that of cells grown in different groups ($p > 0.05$). **c** The cell apoptosis of fibroblast was not significantly different than that of cells grown in different groups ($p > 0.05$)

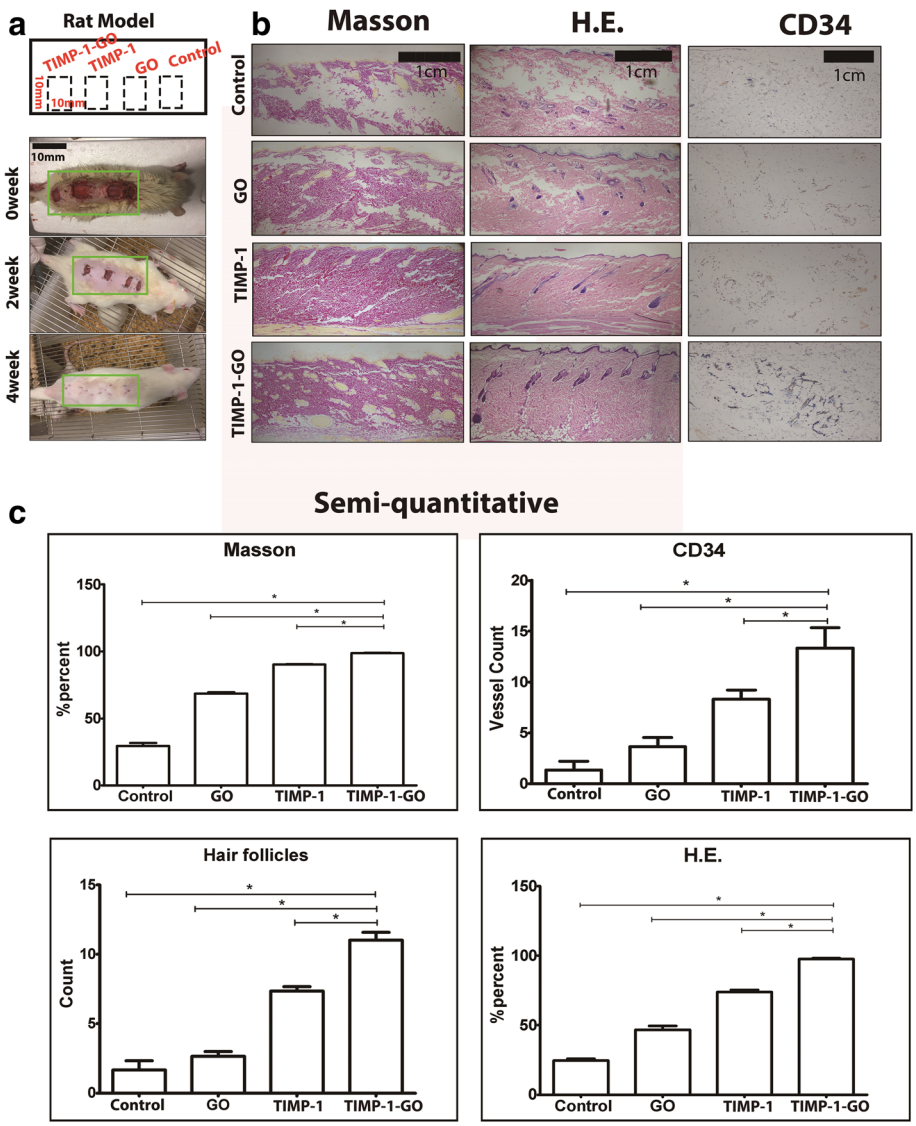

Fig. 4 In vivo experiment. **a** Scheme and the SDS and model. **b** Histologic and immunohistochemical analysis in vivo (1 cm). Continuous collagen fiber is visible in the TIMP-1-GO group. **c** Quantitative assessment revealed significant differences between control and GO compared with TIMP-1 and TIMP-1-GO ($p < 0.05$). The hair follicles of different groups were significantly different ($p < 0.05$). Skin defects treated with TIMP-1 showed significant differences with control group and GO group by semi-quantitative ($p < 0.05$)

shown to promote the vascularization and collagen regeneration in an experimental skin defect model.

A variety of biomedical materials have been evaluated as therapy vehicles for the delivery of agents in tissue regeneration. Vehicles such as collagen, silk, titanium, calcium phosphate cement, and polylactic acid-polyglycolic acid tend to produce a rapid release of biological agent that may be undesired in some therapy settings [23]. Therefore, the ability of a biomedical vector to provide a slow continuous release of biological molecules can be seen as an important feature. A requirement for this quality is a flexible used to load the drug with the help of an electric charge [24]. Graphene oxide (GO) provides an "off-start" effect that has shown utility for the slow release of various biologic agents both in vitro and in vivo [25–27]. Here, we showed that GO can be used to exert a sustained release of recombinant human TIMP-1 protein. The interaction between hydrophobic π domains of GO and electrostatic interaction can activate the negatively charged domains of GO and allow efficient TIMP-1 protein absorption to GO via the inner hydrophobic regions. The long release of TIMP-1 from GO is ideally suitable for the necessary revascularization in dermal wound repair.

It is suggested that carbon particles with a concentration of more than 50 mg/ml might be deposited in

tissues [28]. Wang et al. suggested that this may cause inflammatory reactions due to its extremely small diameter yet a large functional surface area of GO [29]. In contrast to previous studies, GO deposition was not detected in our study. Given the lack of an obvious side effect seen here, the potential negative of GO nanoparticles cannot be supported. Further studies have suggested on graphene including biological response and safety test [30].

The research on the effect of the interaction of the graphene oxide on cells is an important issue. Graphene is a newly developed biomedical material whose properties suggest its use in many biological applications. However, the potential biology of two-dimensional carbon structure/graphene toxicology and general biological interactions are not fully understood, which will require extensive additional studies.

Conclusion

Graphene oxide (GO) shows sustained biocompatibility when used as a vehicle for the slow delivery of recombinant TIMP-1. TIMP-1 is shown to be continuously released from GO for up to 40 days, and the combination of TIMP-1 with GO is shown to promote the revascularization and collagen regeneration in a model of skin regeneration.

Acknowledgements

The authors have financial support from Zhejiang Province Key Science and Technology Innovation Team (Grant No. 2013TD13), Zhejiang Provincial Natural Science Foundation of China (Grant No. LQ16H160006), and National Science Foundation for Distinguished Young Scholars of China (Grant No. 81601710).

Authors' Contributions

CZ and DS did the animal experiment. CZ and QB drafted the manuscript and carried out most of the analyses. XL and QB participated in the design of the study. YZ and QB conceived and coordinated the study. PJN revised the manuscript for English language correctness. All authors have read and approved the final manuscript.

Ethics approval and consent to participate

All experimental procedures were conducted according to the guidelines of the NIH in the USA. The animals for experimental procedures were approved by the Zhejiang University Ethics Committee.

Competing Interests

The authors declare that they have no competing interests.

Publisher's Note

Springer Nature remains neutral with regard to jurisdictional claims in published maps and institutional affiliations.

Author details

[1]Department of Orthopaedics, First Affiliated Hospital, School of Medicine, Zhejiang University, Hangzhou, China. [2]Department of General Surgery, Second Affiliated Hospital, School of Medicine, Zhejiang University, Hangzhou, China. [3]Medizinische Klinik und Poliklinik IV, Campus Innenstadt, Clinics of University of Munich, Clinical Biochemistry Group, Schillerstr 42, 80336 Munich, Germany. [4]Department of Plastic and Reconstructive Surgery, Second Affiliated Hospital, School of Medicine, Zhejiang University, Hangzhou, China. [5]Institute of Gastroenterology, Zhejiang University, Hangzhou, China.

Received: 4 April 2017 Accepted: 5 September 2017
Published online: 15 September 2017

References

1. Kreutzer C, von Gregory HF, Fischer H (2014) Skin-fat-graft: a simple tool for reconstruction of small deep defects of the nose. Facial Plastic Surgery : FPS 30(3):247–259
2. Wang L, Li L, Lou W (2015) Repair of a cervical skin defect using xenogeneic acellular dermal matrix in a patient with advanced laryngeal carcinoma. J Laryngol Otol 129(7):715–717
3. Wang NZ, Shen ZY, Ma CX (2000) Application of skin and soft tissue expansion in treatment of burn injury. Zhongguo xiu fu chong jian wai ke za zhi = Zhongguo xiufu chongjian waike zazhi = Chinese journal of reparative and reconstructive surgery 14(5):286–289
4. Honore PM, Spapen HD (2016) The struggle to differentiate inflammation from infection in severely burned patients: time to send better biomarkers into the arena? Crit Care 20:13
5. Huang X, Long J, Xie T, Zhang M, Zhang P, Yang X et al (2002) The repair of bulky tissue defect of forearm with skin flaps. Zhonghua shao shang za zhi = Zhonghua shaoshang zazhi = Chinese journal of burns 18(6):334–335
6. Pulz LH, Barra CN, Kleeb SR, Xavier JG, Catao-Dias JL, Sobral RA, Fukumasu H, Strefezzi RF (2017) Increased expression of tissue inhibitor of metalloproteinase-1 correlates with improved outcome in canine cutaneous mast cell tumours. Vet Comp Oncol 15(2):606–614
7. Bao Q, Niess H, Djafarzadeh R, Zhao Y, Schwarz B, Angele MK et al (2014) Recombinant TIMP-1-GPI inhibits growth of fibrosarcoma and enhances tumor sensitivity to doxorubicin. Target Oncol 9(3):251–261
8. Clark IM, Swingler TE, Sampieri CL, Edwards DR (2008) The regulation of matrix metalloproteinases and their inhibitors. Int J Biochem Cell Biol 40(6–7):1362–1378
9. Urbaniak-Kujda D, Kapelko-Slowik K, Prajs I, Dybko J, Wolowiec D, Biernat M et al (2016) Increased expression of metalloproteinase-2 and -9 (MMP-2, MMP-9), tissue inhibitor of metalloproteinase-1 and -2 (TIMP-1, TIMP-2), and EMMPRIN (CD147) in multiple myeloma. Hematology 21(1):26–33
10. Xu R, Xia H, He W, Li Z, Zhao J, Liu B et al (2016) Controlled water vapor transmission rate promotes wound-healing via wound re-epithelialization and contraction enhancement. Sci Rep 6:24596
11. Patel S, Maheshwari A, Chandra A (2016) Biomarkers for wound healing and their evaluation. J Wound Care 25(1):46–55
12. Garash R, Bajpai A, Marcinkiewicz BM, Spiller KL (2016) Drug delivery strategies to control macrophages for tissue repair and regeneration. Exp Biol Med 241(10):1054–1063
13. Ru G, Han L, Qing J, Sheng J, Li R, Qiu M et al (2016) Effects of borneol on the pharmacokinetics of 9-nitrocamptothecin encapsulated in PLGA nanoparticles with different size via oral administration. Drug delivery:1–7
14. Assa F, Jafarizadeh-Malmiri H, Ajamein H, Vaghari H, Anarjan N, Ahmadi O et al (2016) Chitosan magnetic nanoparticles for drug delivery systems. Crit Rev Biotechnol:1–18
15. Vega E, Gamisans F, Garcia ML, Chauvet A, Lacoulonche F, Egea MA (2008) PLGA nanospheres for the ocular delivery of flurbiprofen: drug release and interactions. J Pharm Sci 97(12):5306–5317
16. Sui S, Wang Y, Kolewe KW, Srajer V, Henning R, Schiffman JD, Dimitrakopoulos C, Perry SL (2016) Graphene-based microfluidics for serial crystallography. Lab chip 16(16):3082–96
17. McCallion C, Burthem J, Rees-Unwin K, Golovanov A, Pluen A (2016) Graphene in therapeutics delivery: problems, solutions and future opportunities. Eur J Pharm Biopharm 104:235–250
18. Zhong C, Feng J, Lin X, Bao Q (2017) Continuous release of bone morphogenetic protein-2 through nano-graphene oxide-based delivery influences the activation of the NF-kappaB signal transduction pathway. Int J Nanomedicine 12:1215–1226
19. Wu C, Zhang Y, Wu X, Yang Y, Zhou X, Wu H (2012) Biological applications of graphene and graphene oxide. Nano Biomed Eng. 4(4):157–162
20. Reiner-Rozman C, Kotlowski C, Knoll W (2016) Electronic biosensing with functionalized rGO FETs. Biosensors 6(2):17
21. Narayanaswamy V, Qurishi Y, Srivastava C (2017) GO-Fe3O4 nanoparticle composite for selective targeting of cancer cells. Nano Biomed Eng 9(1):96–102

22. Debels H, Gerrand YW, Poon CJ, Abberton KM, Morrison WA, Mitchell GM (2017) An adipogenic gel for surgical reconstruction of the subcutaneous fat layer in a rat model. J Tissue Eng Regen Med 11(4):1230–1241
23. Tan JM, Karthivashan G, Abd Gani S, Fakurazi S, Hussein MZ (2016) Biocompatible polymers coated on carboxylated nanotubes functionalized with betulinic acid for effective drug delivery. Journal of Materials Science Materials in Medicine 27(2):26
24. Kirkpatrick DC, Wightman RM (2016) Evaluation of drug concentrations delivered by microiontophoresis. Anal Chem 88(12):6492–6499
25. Pereira de Sousa I, Buttenhauser K, Suchaoin W, Partenhauser A, Perrone M, Matuszczak B et al (2016) Thiolated graphene oxide as promising mucoadhesive carrier for hydrophobic drugs. Int J Pharm 509(1–2):360–367
26. Khatun Z, Nurunnabi M, Nafiujjaman M, Reeck GR, Khan HA, Cho KJ et al (2015) A hyaluronic acid nanogel for photo-chemo theranostics of lung cancer with simultaneous light-responsive controlled release of doxorubicin. Nano 7(24):10680–10689
27. Cheon YA, Bae JH, Chung BG (2016) Reduced graphene oxide nanosheet for chemo-photothermal therapy. Langmuir : the ACS journal of surfaces and colloids 32(11):2731–2736
28. Li Y, Wu Q, Zhao Y, Bai Y, Chen P, Xia T et al (2014) Response of microRNAs to in vitro treatment with graphene oxide. ACS Nano 8(3):2100–2110
29. Wang X, Podila R, Shannahan JH, Rao AM, Brown JM (2013) Intravenously delivered graphene nanosheets and multiwalled carbon nanotubes induce site-specific Th2 inflammatory responses via the IL-33/ST2 axis. Int J Nanomedicine 8:1733–1748
30. Podila R, Moore T, Alexis F, Rao A (2013) Graphene coatings for biomedical implants. Journal of Visualized Experiments : JoVE 73:e50276

Submit your manuscript to a SpringerOpen journal and benefit from:

► Convenient online submission
► Rigorous peer review
► Open access: articles freely available online
► High visibility within the field
► Retaining the copyright to your article

Submit your next manuscript at ► springeropen.com